Microsyst Technol (2012) 18:1807–1814
DOI 10.1007/s00542-012-1486-0

TECHNICAL PAPER

Study of black silicon obtained by cryogenic plasma etching: approach to achieve the hot spot of a thermoelectric energy harvester

K. N. Nguyen · D. Abi-Saab · P. Basset · E. Richalot · M. Malak · N. Pavy · F. Flourens · F. Marty · D. Angelescu · Y. Leprince-Wang · T. Bourouina

Received: 14 July 2011 / Accepted: 9 March 2012 / Published online: 28 March 2012
© Springer-Verlag 2012

Abstract In this paper, we study the enhanced absorption properties of micro/nano structured silicon surface under incident electromagnetic illumination and its capacity to convert light into heat. We simulate the optical reflectance of three-dimensional micro/nano silicon cones of different dimensions and under different electric field incident angles (θ_i). According to the favorable simulation results, we fabricate black silicon with conical microstructures that exhibits excellent anti-reflectivity behavior. Plasma etching under cryogenic temperatures is used for this purpose in an inductively coupled plasma-reactive ion etching reactor. The reflectance of the black silicon is measured to be approximately 1 % in the optical wavelength range, by using an integrating sphere coupled to a calibrated spectrometer. Furthermore, a device integrating a resistance temperature detector in a black silicon area is developed in order to investigate its efficiency as a photo-thermal converter.

This work was originally presented in the conference DTIP 2011.

K. N. Nguyen (✉) · D. Abi-Saab · P. Basset · M. Malak · N. Pavy · F. Flourens · F. Marty · D. Angelescu · T. Bourouina
ESYCOM, ESIEE Paris, Université Paris-Est,
2 Bd. Blaise Pascal, 93162 Noisy-le-Grand, France
e-mail: k.nguyen@esiee.fr

D. Abi-Saab
e-mail: abisaabd@esiee.fr

P. Basset
e-mail: p.basset@esiee.fr

M. Malak
e-mail: malakkam@esiee.fr

N. Pavy
e-mail: n.pavy@esiee.fr

F. Flourens
e-mail: f.flourens@esiee.fr

F. Marty
e-mail: f.marty@esiee.fr

D. Angelescu
e-mail: d.angelescu@esiee.fr

T. Bourouina
e-mail: t.bourouina@esiee.fr

E. Richalot
ESYCOM, Université Paris-Est, 5 Bd. Descartes,
77454 Marne-la-Vallée Cedex 2, France
e-mail: elodie.richalot@univ-mlv.fr

Y. Leprince-Wang
LPMDI, Université Paris-Est, 5 Bd. Descartes,
77454 Marne-la-Vallée Cedex 2, France
e-mail: yamin.leprince@univ-mlv.fr

1 Introduction

Significant research in the area of electromagnetic energy harvesting has been performed over the past decades. In the optical wavelength range, one can use photovoltaic conversion (Böhm et al. 1984; Nijs et al. 2001; Ruby et al. 2002; Lee et al. 2007; Catchpole and Polman 2008) as well as photo-thermal conversion (Booth et al. 1979; Bogaerts and Lampert 1983; Garnich and Sailer. 1990; Sai et al. 2003); the efficiencies of each conversion technique depend on the material properties. Either mechanism is possible on silicon, with various efficiencies depending on the doping level and the wavelength of incident light (Bogaerts and Lampert 1983; Vetterl et al. 2000). Also, microstructuring the surface of silicon can lead to noticeable enhancement of conversion efficiency (Manea et al. 2006; Yoo et al. 2009).

In this paper we study the photo-thermal conversion behavior of black silicon obtained by cryogenic plasma

etching, with the prospect of producing a hot spot intended to integrate a thermoelectric energy harvester consisting of a vertical superlattice (Parasuraman et al. 2010). In order to fuel such thermoelectric elements by solar radiation, the optimization of the hot spot is crucial. To this end, we propose in this paper to develop a light-absorbing layer with extremely low reflectance so as to maximize heating of the hot spot under the effect of electromagnetic (EM) radiation in the visible and near-infrared ranges. The hot spot is made of black silicon, a material consisting of dense (sub)-micrometer cones which lead to multiple reflections of incident photons and hence to light trapping and enhanced absorption. A 3D model of our target device is shown in Fig. 1b is the AA′ cut view of the 3D image. An air cavity etched on the back side thermally insulates the hot spot, which is heated by incident light focused by a microlens.

Silicon remains the most widely used substrate material in microtechnology thanks to the availability of the processing facilities and its reduced cost. The natural reflectance of a flat silicon/air interface is around 30 % because of the high refractive index of silicon ($n_{Si} \sim 3.48$). Surface texturing is an effective technique to reduce the reflectance of the Si surface. Several techniques have been previously studied for forming different profiles such as wet etching (Manea et al. 2006; Branz et al. 2009), femtosecond laser pulses (Shen et al. 2004), reactive ion etching (Damiani et al. 2000; Yoo et al. 2009) and inductively coupled plasma-reactive ion etching (ICP-RIE), also referred as to deep reactive ion etching (DRIE) (Jansen et al. 2001; De Boer et al. 2002; Marty et al. 2005). Maskless texturing of a polished silicon wafer can result in the formation of "grass"-like structures (Fig. 1c) that appears black to the human eye, hence the name "black silicon" (Damiani et al. 2000; Jansen et al. 2001). Plasma texturing using DRIE is a well-known technique to obtain black silicon surfaces of low reflectance. The DRIE is based on inductively coupled plasma (ICP) of sulphur hexafluoride (SF_6) and allows anisotropic etching of silicon by taking advantage of a passivation mechanism in the side walls. While the so-called "Bosch" technique is the most widely used process in DRIE mainly for the purpose of obtaining high aspect ratio structures with vertical sidewalls, we have privileged in this work the cryogenic process to obtain black silicon surfaces.

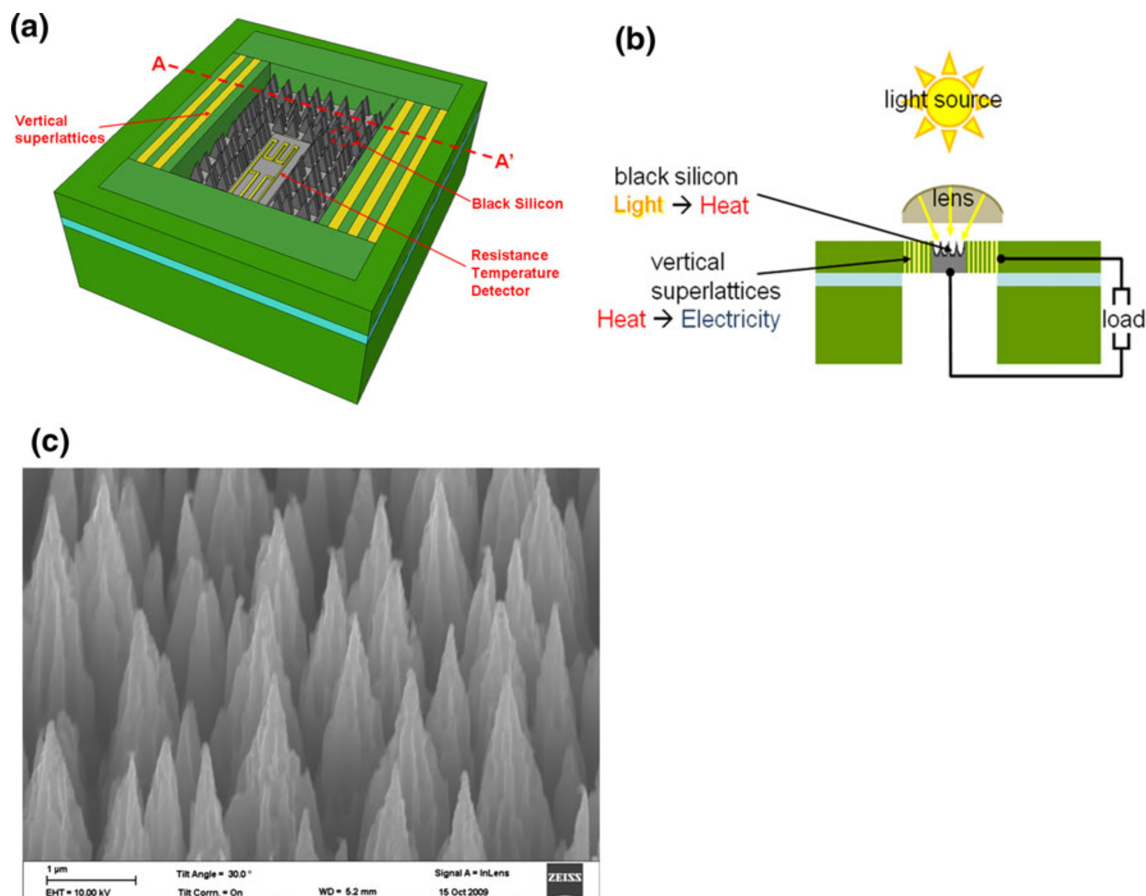

Fig. 1 **a** 3D sketch of the target material. **b** Cut view AA′ of the 3D sketch of the target material. **c** Scanning electron microscope image of a typical black silicon area obtained by a cryogenic plasma process

2 FEM electromagnetic simulations of black silicon reflectance

The influence of process parameters on the black silicon structure has been actively studied (Jansen et al. 2001) but to the best of our knowledge, no in-depth study concerning the impact of its 3D geometry on the reflectance of the incident EM radiation has been done. Hence, simulations of the reflectance of a model for the black silicon surface are performed with ANSOFT High Frequency Structural Simulator (HFSS) software based on the Finite Element Method (FEM). Although black silicon can be built in various shapes such as spikes, "penguin-like" structures, columns and pyramids, the simulations are performed with cones since it is one of the shapes that provides better absorption (Halbwax et al. 2008). In this paper, we focus on textured surfaces formed by cones of dimensions (height and width) varying between 150 nm and 5 µm under different directions of the incident field.

2.1 Description of the 3D surface

The 3D simulated structure consists of a silicon substrate on which identical cones are periodically repeated along the *x*- and *y*-axis. The structure is defined by its out-of-plane height (*h*), base diameter (*d*), and in-plane periodicity (*p*), as represented in Fig. 2. According to Floquet's theorem (Petit 1980), the structure periodicity induces the field pseudo-periodicity and allows us to reduce the computation time by restricting it to a single lattice unit with bi-periodic boundary conditions (Richalot et al. 2000). The surface is excited by an incident monochromatic plane wave with a wavelength tuned from 430 to 1,000 nm. The reflectance is obtained by calculating the ratio between the reflected and incident energies passing through a surface *S*. The surface *S* has the same dimensions as the elementary cell and is placed above the simulated cone and parallel to the periodicity plane.

3 Results

3.1 Influence of the height of cones

To evaluate the influence of cone height on the reflectance of black silicon, we have simulated a structure with identical cones of varying height. The periodicity and the width of cones are of 1.5 µm while the height is varied from 3.5 to 5 µm. This structure is illuminated in a direction normal to the substrate. The results given in Fig. 3a show that the reflectance in the visible light range decreases uniformly while increasing cone height due to multiple reflections of the incident light on the silicon 3D surface. Now if we compare the curves obtained at different wavelengths while increasing cone height of this structure (Fig. 3b), we observe that while the dependence of reflectance on height is modest in the infrared limit (1,000 nm), it is significant at lower wavelengths (430–600 nm).

3.2 Influence of the diameter of cones

The impact of the cone diameter on the reflectance is studied by simulating micrometer size cones of constant periodicity ($p = 1.5$ µm) and height ($h = 3.5$ µm), whose diameter is varied from 1 to 2.08 µm. In this case, normal incidence is considered. The simulated reflectance of these structures is shown in Fig. 4. It appears that at constant periodicity, the reflectance decreases with increasing cone diameter when the diameter is lower than the periodicity. The curve slope decreases from the point where the bases of the structure are in contact. The very large decrease in reflectance prior to this point can be understood by the large reduction of the planar surface between the cones. Then the cone bases start to overlap. Before the planar surface disappears completely, the reflectance starts to increase slightly, which can then be explained by the reduction of the angle between the incident field and the normal of the cone lateral surface, and by the induced

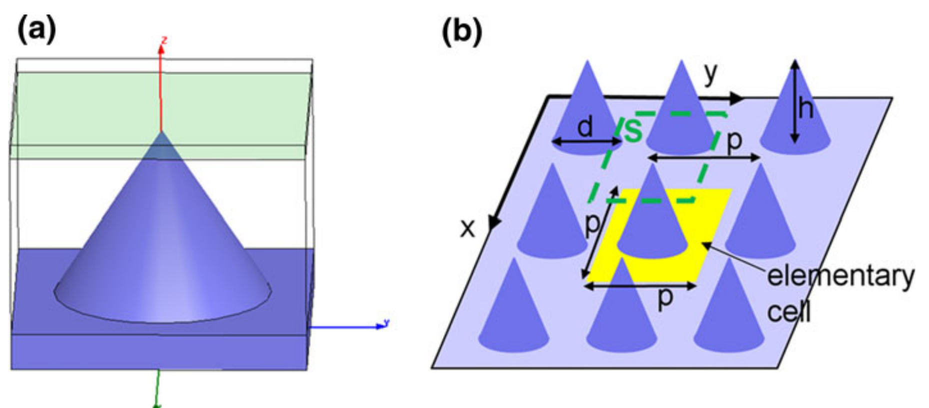

Fig. 2 **a** Diagram of the elementary cell simulated by HFSS™. **b** 3D sketch of the simulated surface

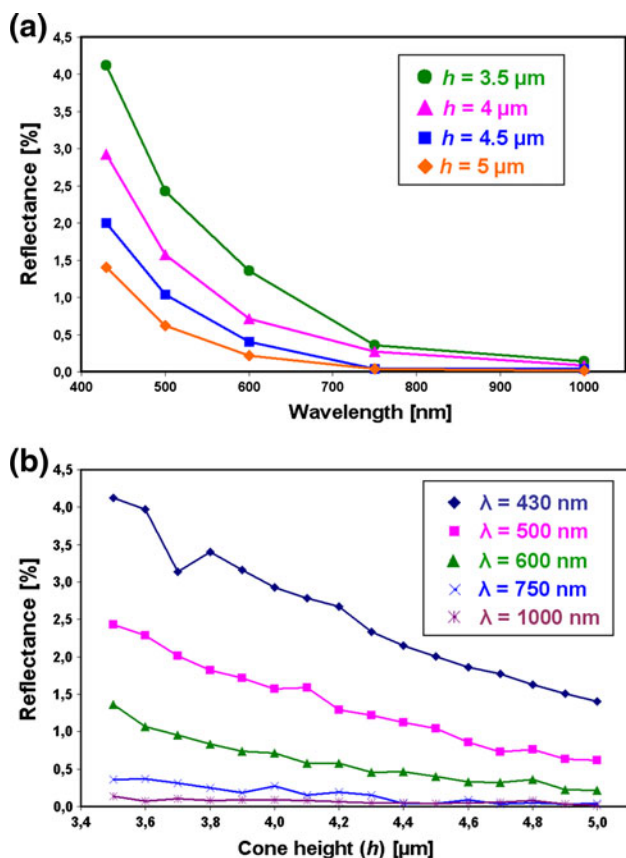

Fig. 3 **a** Simulated reflectance for conical structure ($p = 1.5$ µm, $d = 1.5$ µm) with varying cone height (h). **b** Comparison of the reflectance at different wavelengths for conical structure ($p = 1.5$ µm, $d = 1.5$ µm) with varying cone height (h)

reduction of the cone aspect ratio. We observe that the lowest reflectance is obtained for a cone diameter approximately 30 % larger than the structure periodicity.

3.3 Influence of the incident electric field angle

Since promising results on the physical parameters of silicon conical structures for the lowest reflectance are found as mentioned above, textured surfaces consisting of micrometer and sub-micrometer cones with high steepness and high density are simulated to study the variation of the reflectance with respect to the incident field direction. Fresnel's Equation (1) is used as a reference for the variation of the reflected field on a theoretical polished surface silicon wafer.

$$R_s(\lambda) = \left(\frac{n_1(\lambda)\cos\theta_i - n_2(\lambda)\sqrt{1 - \left(\frac{n_1(\lambda)}{n_2(\lambda)}\sin\theta_i\right)^2}}{n_1(\lambda)\cos\theta_i + n_2(\lambda)\sqrt{1 - \left(\frac{n_1(\lambda)}{n_2(\lambda)}\sin\theta_i\right)^2}} \right)^2 \quad (1)$$

where R_s is the s-polarized reflection coefficient, λ is the wavelength, n_1 and n_2 are the refraction index of air and silicon respectively, θ_i is the incident field angle from the normal incidence. Simulations are performed with the variation of θ_i from 0° to 85° on a planar and textured silicon surface. The periodicity, diameter and height of sub-micrometer cones are 150, 190 and 910 nm respectively. The light reflection of polished silicon and the conical structured black silicon at 600 nm with respect to the different incident angles is given in Fig. 5. As shown in Fig. 6, we can notice that high density cones exhibit a low reflectance in the visible range for incidence angles up to 45° with respect to the normal on the surface. A similar effect is observed for the micrometer size structures whose dimensions are presented in Fig. 4.

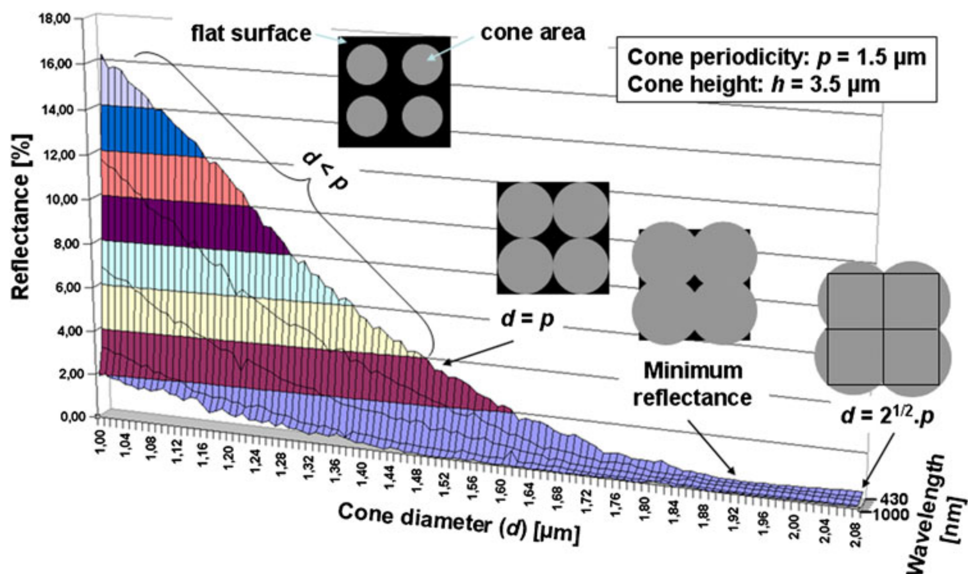

Fig. 4 Cone width influence on simulated reflectance

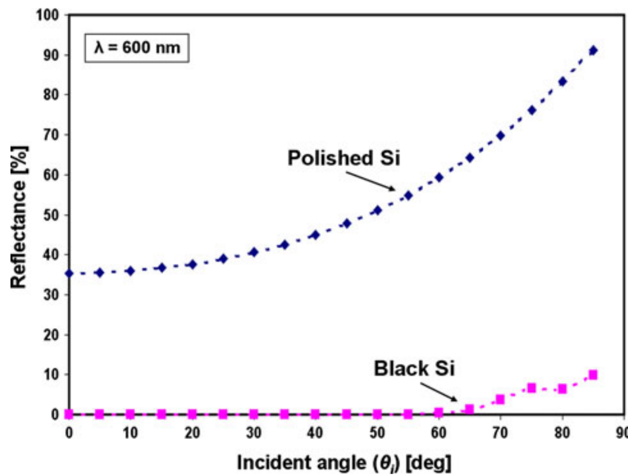

Fig. 5 Simulated reflectance of planar silicon surface and conical structure ($p = 150$ nm, $d = 190$ nm, $h = 910$ nm) with respect to the electric field incident angle at 600 nm

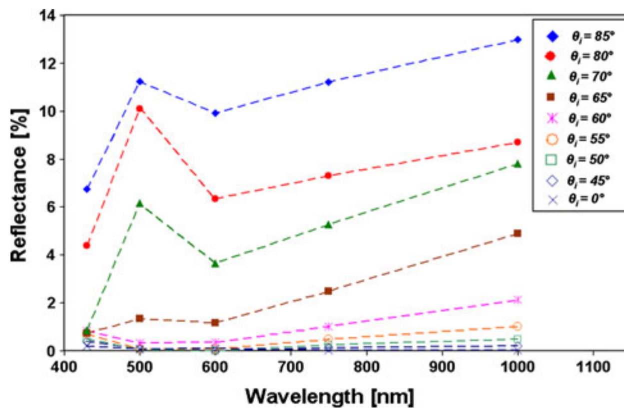

Fig. 6 Example of simulated reflectance with respect to the electric field incident angle θ_i, for a biperiodic conical structure ($p = 150$ nm, $d = 190$ nm, $h = 910$ nm). These results predict sub-percent reflectances at $\theta_i < 55°$

4 Experimental results

4.1 Sample fabrication

Herein, we report about the fabrication process used to develop the photo-thermal test device. The considered device contains a hot spot of black silicon fabricated on a finite silicon surface whose center integrates a thin film of platinum acting as a resistance temperature detector (Pt RTD) in order to investigate the photo-thermal conversion of the black silicon. Platinum was used because of its stability, precision and the linear relationship that it exhibits between resistance and temperature. The relation between them for the temperature above 0 °C is as follows:

$$R(T) = R(0) \times (1 + A \times T) \quad (2)$$

where $R(T)$ and $R(0)$ are respectively the resistance at temperature T and at 0 °C; A is the temperature coefficient resistance (TCR) of platinum and is equal to 3,850 ppm/°C. The main process steps used to realize the test device are described in Fig. 7. Silicon on insulator (SOI) wafer was employed as well to achieve this process. Firstly, a thermal silicon oxide layer, used as a dielectric passivation layer, was created on the silicon substrate. Following the photolithography step, a sandwich of Ti/Pt layers (20 nm/150 nm) was deposited by sputtering and then patterned by lift-off. The Ti layer was used to enhance the adhesion of Pt on the silicon dioxide. The Pt RTD was protected by a photoresist layer and then SiO_2 was etched by SF_6/CHF_3 based RIE process. Lastly, the black silicon was obtained using O_2–SF_6 cryogenic DRIE and the photoresist layer is removed by O_2 plasma. For the black silicon cryogenic process, by varying the process parameters such as bias voltage, temperature, gas pressure, and RF power, one can obtain various structure geometries (Dussart et al. 2005; Henry et al. 2009). The wafers were subjected to DRIE at cryogenic temperatures (T $\sim$ −110 °C) without any mask. SF_6 gas generates $F^{\cdot}$ radicals for chemical etching of silicon leading to volatile SiF_4 whereas O_2 gases produce $O^{\cdot}$ radicals for silicon sidewall passivation with $Si_xO_yF_z$. Such wafers were treated under different plasma conditions in order to obtain different textures of black silicon. Depending of the process conditions, substrates with micrometer (Fig. 1c) as well as sub-micrometer (Fig. 8) cones have been obtained. The black silicon in Fig. 8 was fabricated on a surface area of 36 mm^2 for the photo-thermal test device. A thin film Pt RTD at micrometer scale was designed and realized to measure its temperature change under exposure to various intensities of light and further absorption by the surrounding black silicon (Fig. 9). A four probe resistance measurement was performed to eliminate contact resistances and increase the accuracy of the measurement.

4.2 Characterization

According to the FEM simulation results, the black silicon structure with lowest reflectivity should have high density and sharpest cones. This result has been confirmed experimentally in (Nguyen et al. 2011) but the black silicon cryogenic process is hardly fully reproducible (Sainiemi et al. 2011). In the test device with integrated RTD, the cones have an average width of 350 nm and an average height of 1.4 µm, which were directly extracted from side-view scanning electron microscopy (SEM) image (Fig. 8). The Fourier transform (FT) was performed on the top view SEM to extract the pseudo-periodicity of the cones.

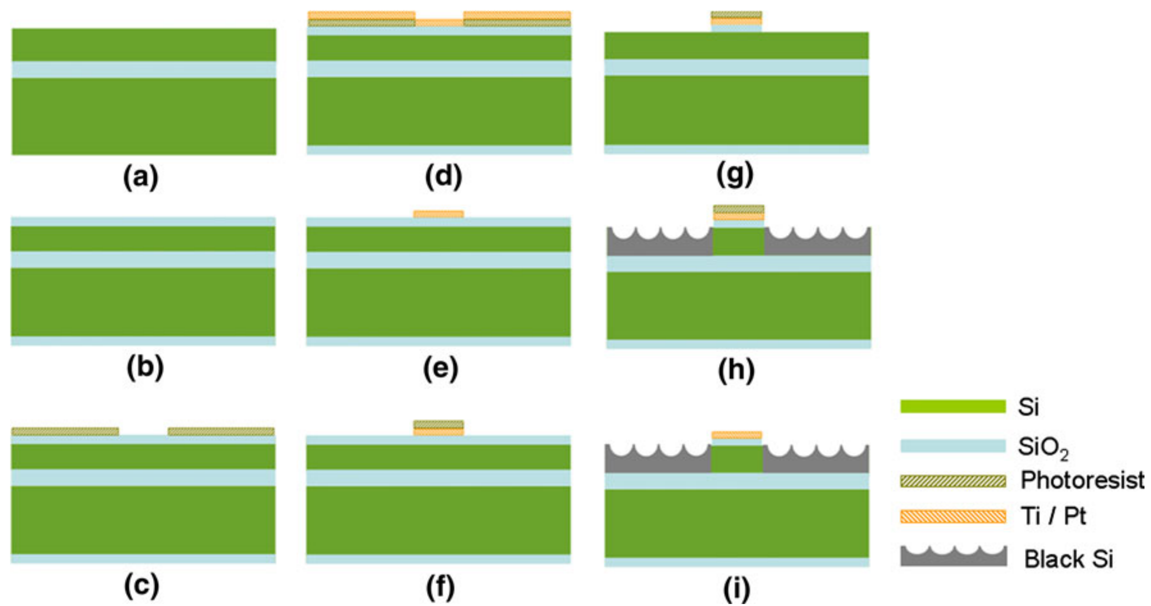

Fig. 7 Schematic process for the fabrication of the photo-thermal tested device **a** SOI substrate, **b** thermal oxide deposition, **c** photolithography, **d** Ti/Pt sputtering deposition, **e** lift-off, **f** photolithography, **g** SiO_2 etching, **h** cryogenic DRIE, **i** photoresist removal

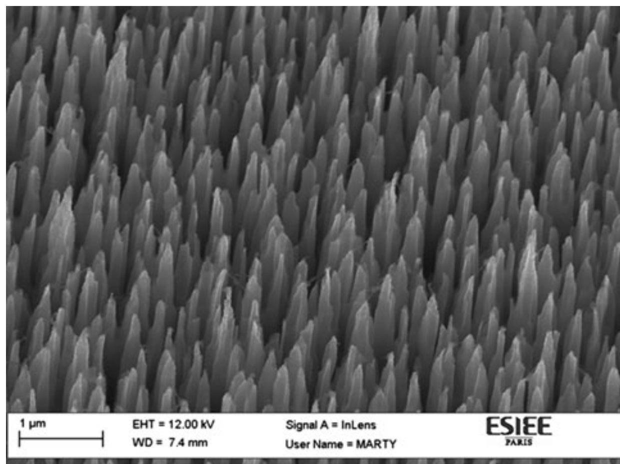

Fig. 8 SEM image of black Si obtained by a cryogenic DRIE process for the photo-thermal test device

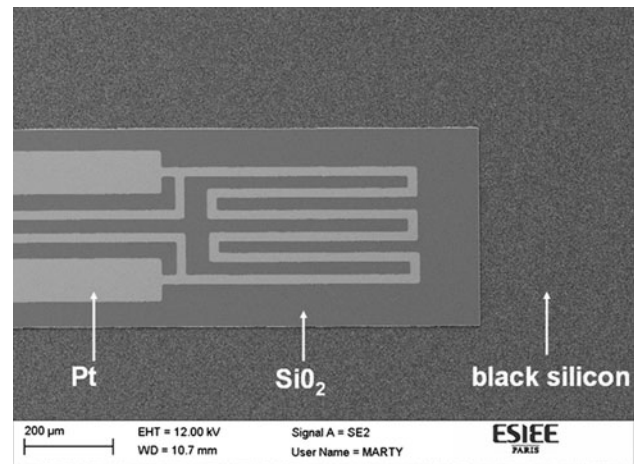

Fig. 9 SEM image of a platinum (Pt) resistance temperature detector (RTD) surrounded by black silicon

As the surface properties of the black silicon are spatially invariant, the FT image is symmetrical to the centre. Then, Matlab is used to calculate the average intensity of all points at a radius (r) over 360° as given in Eq. (3):

$$I_{average} = \frac{\int_0^{2\pi} f(r,\theta)d\theta}{2\pi r} \quad (3)$$

The radius r, associated with the maximum of the azimuthal average, corresponds to the image mean periodicity (see Fig. 10). The average periodicity of this structure is then calculated as 570 nm.The reflectance of black silicon has been measured for wavelengths between 400 and 1,000 nm by a spectrometer (Maya 2000 Pro from Ocean Optic) with an integrating sphere coupled to a halogen light source. NIST-accredited reflectivity standards were used for calibration. The graph in Fig. 11 shows the measured reflectance spectrum from planar and DRIE-textured surface under normal incidence. This black silicon is found to exhibit a reflectance of $\sim$1 % in the visible range without anti-reflection films.

Then, the device was tested by irradiating it with different intensities of visible light coming from a halogen light source. The resistance variation (Fig. 12) $\Delta R/R$ is nearly 7,000 ppm for an incident light intensity of 1.6 mW/mm^2

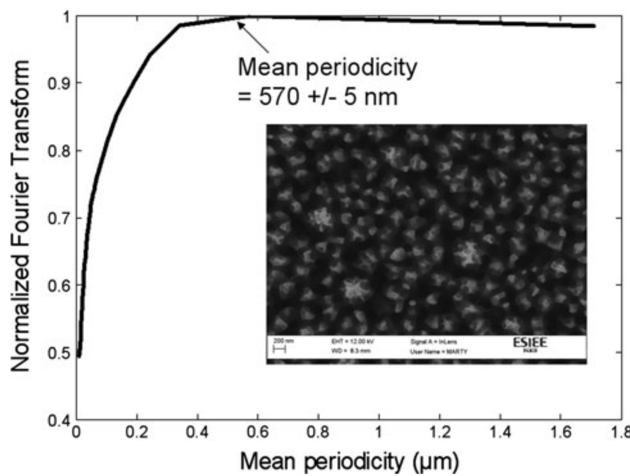

Fig. 10 Top view SEM image of black Si of Fig. 8 and azimuthal average of the Fourier transform of the top view image, revealing an average periodicity of 570 nm

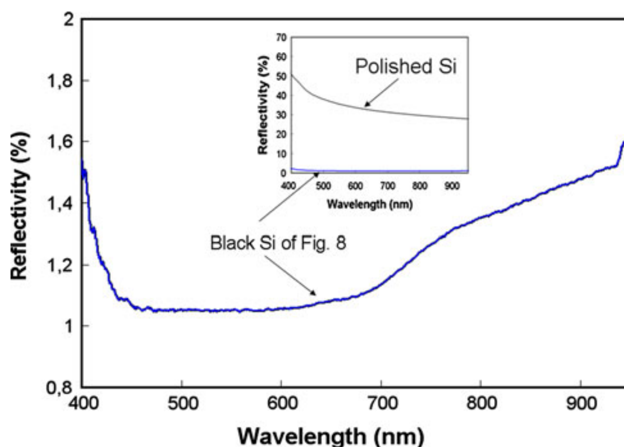

Fig. 11 Measured reflectance spectrum of black silicon of Fig. 8 under normal incidence. The *inset* gives the measured reflectance spectrum of a polished silicon surface, for reference

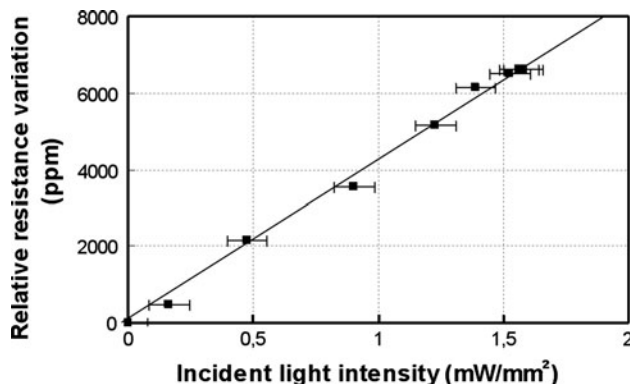

Fig. 12 Resistance variation of the platinum (Pt) resistance temperature detector (RTD) under different incident light power densities

equivalent to a temperature increase of nearly 2 °C and to a photo-thermal conversion of 1,250 °C/W/mm^2 for this device. It is worth mentioning that this first trial was performed on a device suspended on a membrane but with no additional thermal insulation from the thermally conductive substrate.

5 Conclusion

We have simulated the optical reflectance of the 3D black silicon structures consisting of cones of sub-micro and micrometer dimensions with different heights and diameters for the optical wavelengths. We observed that a black silicon structure with the sharpest cones and the highest cone density is expected to provide the lowest reflectance. The optimal cone diameter is about 30 % larger than the periodicity. Besides, the influence of the direction of the incident field on the reflection of black silicon cannot be neglected. It is shown that the angle of the incidence from the normal surface has almost no influence up to 45° on a low reflective surface.

We have fabricated a silicon membrane of black silicon with integrated platinum RTD in order to investigate its photo-thermal conversion efficiency. Conical black silicon was fabricated on a finite surface area of 36 mm^2 around the Pt RTD using DRIE under cryogenic temperatures. This black silicon has a diameter of 350 nm, a height of 1.4 µm and a periodicity of 570 nm. This structure presents excellent antireflective behavior over the 400–950 nm spectral range with a reflectance ~1 % in the visible range. This reflectance level is among the best reported in the literature for plasma batch-fabricated black silicon. We have successfully measured the variation in the photo-thermal effects of black silicon with varying incident light intensities albeit notably without thermal insulation substrates. The current work focuses on improving the prototype for the light-thermal conversion and the thermoelectric conversion.

Acknowledgments The authors would like to thank to EADS Foundation by whom this work is funded through the project TESEER.

References

Bogaerts WF, Lampert CM (1983) Materials for photothermal solar energy conversion. J Mater Sci 18(10):2847–2875. doi:10.1007/BF00700767

Böhm M, Scheer HC, Wagemann HG (1984) A two-dimensional model for polycrystalline silicon solar cells. Sol Cells 13(1):29–41. doi:10.1016/0379-6787(84)90090-5

Booth DC, Allred DD, Seraphin BO (1979) Stabilized CVD amorphous silicon for high temperature photothermal solar

energy conversion. Sol Energy Mater 2(1):107–124. doi:10.1016/0165-1633(79)90034-0

Branz HM, Yost VE, Ward S, Jones KM, To B, Stradinset P (2009) Nanostructured black silicon and the optical reflectance of graded-density surfaces Appl Phys Lett 94(23), art. no. 231121. doi: 10.1063/1.3152244

Catchpole KR, Polman A (2008) Plasmonic solar cells. Opt Express 16(26):21793–21800. doi:10.1364/OE.16.021793

Damiani BM, Lüdemann R, Ruby DS, Zaidi SH, Rohatgi A (2000) Development of RIE-textured silicon solar cells. In: Photovoltaic specialists conference. Conference record of the twenty-eighth IEEE, pp 371–374. doi: 10.1109/PVSC.2000.915843

De Boer MJ, Gardeniers JGE, Jansen HV, Smulders E, Gilde MJ, Roelofs G, Sasserath JN, Elwenspoek M (2002) Guidelines for etching silicon MEMS structures using fluorine high-density plasmas at cryogenic temperatures. J Microelectromech Syst 11(4):385–401. doi:10.1109/JMEMS.2002.800928

Dussart R, Mellhaoui X, Tillocher T, Lefaucheux P, Volatier M, Socquet-Clerc C, Brault P, Ranson P (2005) Silicon columnar microstructures induced by an SF_6/O_2 plasma. J Phys D Appl Phys 38(18):3395–3402. doi:10.1088/0022-3727/38/18/012

Garnich F, Sailer E (1990) Cu-SiO_2/Cu-cermet selective absorbers for solar photothermal conversion. Sol Energy Mater 20(1–2):81–89. doi:10.1016/0165-1633(90)90019-W

Halbwax M, Sarnet T, Delaporte Ph, Sentis M, Etienne H, Torregrosa F, Vervisch V, Perichaud I, Martinuzzi S (2008) Micro and nano-structuration of silicon by femtosecond laser: application to silicon photovoltaic cells fabrication. Thin Solid Films 516(20): 6791–6795. doi:10.1016/j.tsf.2007.12.117

Henry MD, Welch C, Scherer A (2009) Techniques of cryogenic reactive ion etching in silicon for fabrication of sensors. J Vac Sci Technol A 27(5):1211–1216. doi:10.1116/1.3196790

Jansen H, De Boer M, Wensink H, Kloeck B, Elwenspoek M (2001) The black silicon method VIII. A study of the performance of etching silicon using SF_6/O_2-based chemistry with cryogenical wafer cooling and a high density ICP source. Microelectron J 32(9):769–777. doi:10.1016/S0026-2692(01)00039-8

Lee TY, Alegaonkar PS, Yoo JB (2007) Fabrication of dye sensitized solar cell using TiO_2 coated carbon nanotubes. Thin Solid Films 515(12):5131–5135. doi:10.1016/j.tsf.2006.10.056

Manea E, Budianu E, Purica M, Cernica I, Babarada F (2006) Technological process for a new silicon solar cell structure with honeycomb textured front surface. Sol Energy Mater Sol Cells 90(15):2312–2318. doi:10.1016/j.solmat.2006.03.036

Marty F, Rousseau L, Saadany B, Mercier B, Francais O, Mita Y, Bourouina T (2005) Advanced etching of silicon based on deep reactive ion etching for silicon high aspect ratio microstructures and three-dimensional micro- and nanostructures. Microelectron J 36(7):673–677. doi:10.1016/j.mejo.2005.04.039

Nguyen KN, Abi-Saab D, Basset P, Richalot E, Marty F, Angelescu D, Leprince-Wang Y, Bourouina T (2011) Black silicon with sub-percent reflectivity: influenced of the 3D texturization geometry. In: Transducers 2011, 16th international conference on solid-state sensors, actuators and microsystems

Nijs JF, Szlufcik J, Poortmans J, Sivoththaman S, Mertens RP (2001) Advanced cost-effective crystalline silicon solar cell technologies. Sol Energy Mater Sol Cells 65(1):249–259. doi:10.1016/S0927-0248(00)00100-8

Parasuraman J, Bardoux M, Basset P, Angelescu D, Chantrenne P and Bourouina T (2010) Development of vertical superlattices in silicon for on-chip thermal management. In: Proceedings of the 16th International workshop on thermal investigations of ICs and systems (THERMINIC'10), art. no. 5636317, pp 282–284

Petit R (1980) Electromagnetic theory of gratings. Springer-Verlag, Berlin. ISBN-10:0387101934

Richalot E, Bonilla M, Wong MF, Fouad-Hanna V, Baudrand H, Wiart J (2000) Electromagnetic propagation into reinforced-concrete walls. IEEE Trans Microwave Theory Tech 48(3):357–366. doi:10.1109/22.826834

Ruby DS, Zaidi SH, Narayanan S, Damiani BM, Rohatgi A (2002) RIE-texturing of multicrystalline silicon solar cells. Sol Energy Mater Sol Cells 74(1–4):133–137. doi:10.1016/S0927-0248(02)00057-0

Sai H, Yugami H, Kanamori Y, Hane K (2003) Solar selective absorbers based on two-dimensional W surface gratings with submicron periods for high-temperature photothermal conversion. Sol Energy Mater Sol Cells 79(1):35–49. doi:10.1016/S0927-0248(02)00364-1

Sainiemi L, Jokinen V, Shah A, Shpak M, Aura S, Suvanto P, Franssila S (2011) Non-reflecting silicon and polymer surfaces by plasma etching and replication. Adv Mater 23(1):122–126. doi:10.1002/adma.201001810

Shen MY, Crouch CH, Carey JE, Mazur E (2004) Femtosecond laser-induced formation of submicrometer spikes on silicon in water. Appl Phys Lett 85(23):5694–5696. doi:10.1063/1.1828575

Vetterl O, Finger F, Carius R, Hapke P, Houben L, Kluth O, Lambertz A, Mück A, Rech B, Wagner H (2000) Intrinsic microcrystalline silicon: a new material for photovoltaics. Sol Energy Mater Sol Cells 62(1):97–108. doi:10.1016/S0927-0248(99)00140-3

Yoo J, Yu G, Yi J (2009) Black surface structures for crystalline silicon solar cells. Mater Sci Eng B Solid State Mater Adv Technol 159–160(C):333–337. doi: 10.1016/j.mseb.2008.10.019